

Variable Stiffness for Robust Locomotion through Reinforcement Learning*

*submitted to the 16th IFAC joint symposia of mechatronics and robotics

Dario Spoljaric
Autonomous Systems
TU Wien
Vienna, Austria
dario.spoljaric@tuwien.ac.at

Yan Yashuai
Autonomous Systems
TU Wien
Vienna, Austria
yashuai.yan@tuwien.ac.at

Dongheui Lee
Autonomous Systems, TU Wien
Institute of Robotics and Mechatronics, DLR
Vienna, Austria & Wessling, Germany
dongheui.lee@tuwien.ac.at

Abstract—Reinforcement-learned locomotion enables legged robots to perform highly dynamic motions but often accompanies time-consuming manual tuning of joint stiffness. This paper introduces a novel control paradigm that integrates variable stiffness into the action space alongside joint positions, enabling grouped stiffness control such as per-joint stiffness (PJS), per-leg stiffness (PLS) and hybrid joint-leg stiffness (HJLS). We show that variable stiffness policies, with grouping in per-leg stiffness (PLS), outperform position-based control in velocity tracking and push recovery. In contrast, HJLS excels in energy efficiency. Furthermore, our method showcases robust walking behaviour on diverse outdoor terrains by sim-to-real transfer, although the policy is solely trained on a flat floor. Our approach simplifies design by eliminating per-joint stiffness tuning while keeping competitive results with various metrics.

Index Terms—reinforcement learning, quadruped locomotion, variable stiffness, sim-to-real.

I. INTRODUCTION

Animal and human-like locomotion has a significant advantage over wheeled mobile robots. They can traverse unstructured, challenging terrains. Therefore, various approaches are developed to solve quadrupedal and bipedal locomotion. Conventionally, this involved model-based controllers (Donghyun et al., 2019; Jared et al., 2018) with a complex pipeline that managed gait schedule, state estimation, whole body impulse control and actuator control. Recently, this discipline has made significant progress through model-free reinforcement learning (RL) methods. These approaches enable the design of controllers capable of following high-level commands (walking, running, jumping, etc.) and directly actuating the joint motors, bypassing the need for path planning and other parts within the control pipeline. Usually, these controllers (Shuxiao et al., 2023; Gilbert et al., 2023) follow a position- or torque-based paradigm. The high-level controller (RL agent) learns a position policy in the position-based paradigm. Given the state, the RL agent predicts desired joint positions at low frequencies, which are transferred into torques by a high-frequency PD controller. This control paradigm requires manual engineering of motor stiffness and damping for different tasks. In contrast, humans and animals can adjust their stiffness



Fig. 1: A quadrupedal robot traverses across different terrains with variable-stiffness RL policy.

and damping to handle different tasks. For example, we stiffen our foot joints when landing with a foot but relax in the swing phase. The torque-based control circumvents this by directly learning a torque policy, which shows higher compliance (Donghyeon et al., 2023). Generally, torque-based policies are more challenging to train because they require learning complex dynamics. On the other hand, position control has a good initial pose, easing the learning progress in the beginning. Torque-based RL agents are usually executed at higher speeds, necessitating more powerful hardware or smaller networks. Either additional tuning is required to specify the joint stiffness for each task, or a hard-to-train policy limits the scope of the RL for locomotion, as illustrated in Fig. 1. Videos of the results are available online¹. Another approach (Lei et al., 2024; Jiaming et al., 2024) is variable stiffness control, which is widely used in robotics, particularly in manipulator applications, to improve safety while still being able to track accurately. Preliminary studies from Lei et al., 2024 have shown that applying this technique to locomotion can

¹https://drive.google.com/file/d/1SmwQSM5026Ri41Ue6J_IgP0NqYIFxCOt/view?usp=sharing

enhance energy efficiency. This also seems reasonable as higher stiffness is required during contact with the ground, but less is needed during the swing phase. In quadruped locomotion, research from Xinyuan et al., 2022 within model-based frameworks has shown that variable stiffness can reduce contact forces. However, successfully achieving locomotion with variable stiffness remains a significant challenge. This has motivated the exploration of learning joint stiffness as an integral part of the reinforcement learning process.

This paper studies reinforcement-learned controllers that learn joint stiffness alongside target positions. Consequently, the robot can automatically adjust the motor stiffness according to the task requirements. Our approach shows superior velocity tracking and push recovery performance while maintaining good energy efficiency and robust sim-to-real transfer performance.

II. RELATED WORK

RL has emerged as a promising approach for solving locomotion tasks, offering two primary paradigms: position-based and torque-based control.

Gilbert et al., 2023 and Nahrendra, Yu, and Myung, 2023 predict target joint positions, which are actuated using proportional-derivative (PD) controllers. These methods are widely favoured for their ease of training and robustness in high-level command tracking. Within this control, the torque applied to the motors is calculated using Eq. (1)

$$\tau_t = K_p(q_{t, target}(\theta) - q_t) + K_d(\dot{q}_{des} - \dot{q}_t) \quad (1)$$

However, they suffer from limited compliance behaviour due to fixed stiffness and damping values (K_p and K_d), requiring extensive PD gain tuning that is often task- and robot-specific. Gilbert et al., 2023

In this control, the PD controller acts as a low-level tracking module, where the proportional gain (P-gain) is representative of the stiffness and the derivative gain (d-gain) for the damping. Zhaoming et al., 2021 investigated the impact of the p-gains, suggesting that large proportional gain leads to instabilities in training. In contrast, the low proportional gain has significant tracking errors and behaves like a torque controller. Other research studied the impact on the derivative gain. Laura, Ilya, and Sergey, 2023 showed small derivative gains result in learning instabilities, and large gains prevented tracking the target velocity.

To circumvent this PD controller, Shuxiao et al., 2023 and Donghyeon et al., 2023 studied torque control as an alternative and applied it to quadruped and biped locomotion. In this control, the actions are directly applied to the motors. Although this control showed higher achievable rewards in the long term, it must be executed at higher speeds to perform similarly to position control. It is more difficult to train initially. The higher control speeds limit the design freedom of torque-based controllers.

Xinyuan et al., 2022 showed for model-based control, that adapting stiffness according to the contact force led to sufficient walking for a quadruped on uneven terrains. Miroslav,

Term	Distribution	Units	Operator
Environmental properties			
Payload Mass (trunk)	$\mathcal{U}(-1.0, 3.0)$	kg	additive
Hip Masses	$\mathcal{U}(-0.5, 0.5)$	kg	additive
Ground friction	$\mathcal{U}(0.3, 1.25)$	-	multiplicative
Gravity offset	$\mathcal{U}(-1.0, 1.0)$	m/s ²	additive
Noise in the observation space			
Joint positions	$\mathcal{U}(-0.01, 0.01)$	rad	additive
Joint velocities	$\mathcal{U}(-1.5, 1.5)$	rad/s	additive
Local velocity	$\mathcal{U}(-0.1, 0.1)$	m/s	additive
Local ang. Velocity	$\mathcal{U}(-0.2, 0.2)$	rad/s	additive
Projected gravity	$\mathcal{U}(-0.05, 0.05)$	rad/s ²	additive
System delay	$\mathcal{U}(0.0, 15.0)$	ms	additive

TABLE I: Domain randomisation in simulation

Majid, and Ludovic, 2020 studied the impact of including joint stiffness alongside joint positions. The torque was then calculated by Eq. (2).

$$\tau_t = K_p(\theta)(q_{t, target}(\theta) - q_t) - K_d(\theta)\dot{q}_t \quad (2)$$

Overall, this work did not test their approach to locomotion but showed the superiority of this concept against torque and position control for two scenarios: a single-legged hopper and a manipulator. The single-legged hopper achieved more considerable jumping heights, and the manipulator maintained a continuous contact force during reference motions with the adjustment of the action space. This motivates and applies stiffness alongside joint positions into the action space and applies it to quadruped locomotion.

Building upon the previous works, we investigate the opportunity of joint stiffnesses alongside joint positions in the action space for a reinforcement learning policy applying to quadruped locomotion.

III. METHODS

We aim to train a policy π_θ with parameters θ that can follow high-level velocity commands. The velocity commands include lateral velocity v_{xy}^{cmd} as well as angular rotation speed ω_z^{cmd} . The prediction of joint targets along joint stiffnesses should accomplish this. An overview of our approach is shown in Fig. 2.

A. Training

We train our controllers using Proximal Policy Optimisation (PPO) (Schulman et al., 2017) with 4096 environments in parallel for 2000 epochs. To improve learning efficiency, we apply early termination if the robot's orientation exceeds 90 degrees from its horizontal position, if joint or torque or joint limits are exceeded or if the robot falls onto its hips, trunk, or lidar. The episode lasts 20 seconds, and we sample commands every 5 seconds.

Simulation environment: We use Mujoco-MJX (Emanuel, 2012) as the simulation environment and apply Domain randomisation to achieve a successful sim-to-real transfer. Table I shows the randomised parameters. Additionally, we expose the policies to external pushes applied from random xy directions. The force magnitudes of the pushes are randomised between 50 - 150 N, and the impulse is 8- 15 Ns. The push is

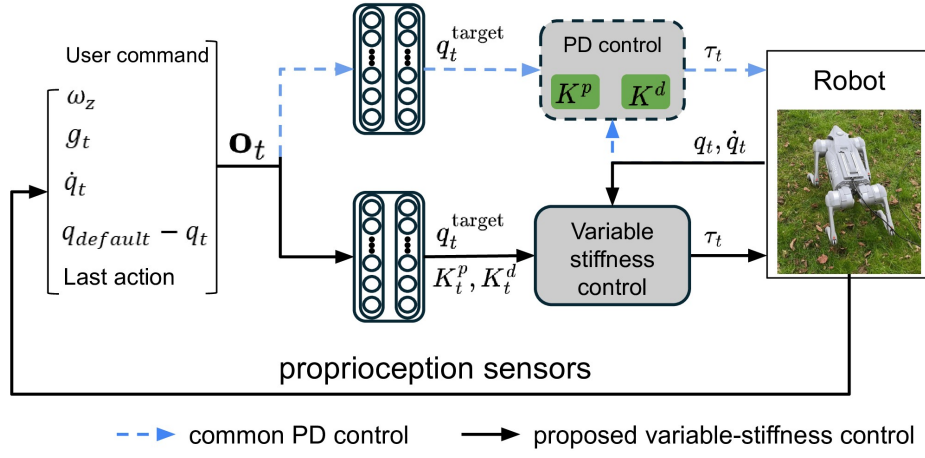


Fig. 2: Variable stiffness concept for quadruped locomotion.

Reward	Equation (r_i)	Weight (w_i)
Lin. velocity tracking	$\exp\left(-4\left(\mathbf{v}_{xy}^{cmd} - \mathbf{v}_{xy}\right)^2\right)$	1.5
Ang. velocity tracking	$\exp\left(-4\left(\omega_{yaw}^{cmd} - \omega_{yaw}\right)^2\right)$	0.8
Linear velocity (z)	v_z^2	-2.0
Angular velocity (xy)	ω_{xy}^2	-0.05
Orientation	\mathbf{s}_{xy}^2	-5.0
Feet air time	$\sum_{f=0}^4 (t_{air,f} - 0.1), \mathbf{v}_{cmd} > 0.1$	0.2
Joint accelerations	\dot{q}^2	-2.5×10^{-7}
Joint power	$ \boldsymbol{\tau} \cdot \dot{\mathbf{q}} $	-2×10^{-5}
Power distribution	$\text{var}(\boldsymbol{\tau} \cdot \dot{\mathbf{q}})$	-10^{-5}
Foot slip	$\sum_{f=0}^4 \ \mathbf{v}_{f,xy}\ ^2, \text{if } z < 0.01$	-0.1
Action rate	$(\mathbf{a}_t - \mathbf{a}_{t-1})^2$	-0.01
Foot clearance	$\sum_{f=1}^4 (\mathbf{p}_{f,z}^{des} - \mathbf{p}_{f,z})^2 v_{f,xy} $	-0.1
Center of mass	$(\mathbf{p}_{com,xy} - \mathbf{p}_{xy}^{des})^2, \mathbf{p}_{xy}^{des} = \frac{\sum_{f=1}^4 \mathbf{p}_{f,xy}}{4}$	-1.0
Joint tracking	$(q_t^{target} - q_{t+1})^2$	-0.1
Base height	$(h^{des} - h)^2$	-0.6
Hip	$\exp\left(-4 * \sum_{k=1}^4 (q_{hip,k} - q_{hip,k}^{default})^2\right)$	0.05
Collisions	$n_{collisions}$	-10.0
Termination	$n_{termination}$	-10.0

TABLE II: Reward functions.

applied every 6 seconds, so the policies have to learn to react to such disturbances. **Observation:** Observations passed to the actor must also be observable during deployment. This limits the freedom of the observations that are passed. The observation vector \mathbf{o}_t , as in Eq. (3), is composed of the body angular velocity in the z-direction $\omega_{z,t}$, projected gravitational vector \mathbf{g}_t , joint angle difference from the default position $\mathbf{q}_t - \mathbf{q}_{default}$, the last action \mathbf{a}_{t-1} and the velocity command \mathbf{c}_t .

$$\mathbf{o}_t = [\omega_{z,t}, \mathbf{g}_t, \mathbf{q}_t - \mathbf{q}_{default}, \dot{\mathbf{q}}_t, \mathbf{a}_{t-1}, \mathbf{c}_t]^T \quad (3)$$

We utilize privileged information to learn the critic network, which is dropped in the inference phase. The privileged vector \mathbf{s}_t consists of the scaling factor for proportional and derivative gains and motor strength σ_t . In addition, \mathbf{s}_t contains ground friction, adapted masses, disturbance force, and regular observation, as stated in Eq. (4).

$$\mathbf{s}_t = [k_{p,t}, k_{d,t}, \sigma_t, \mu, m_t, \mathbf{F}_{kick}, \mathbf{o}_t]^T \quad (4)$$

Reward: The reward functions, similar to Nahrendra, Yu, and Myung, 2023; Rudin et al., 2022; Miroslav, Majid, and

Ludovic, 2020, consist of task rewards to follow the command given and auxiliary rewards (penalties) to stabilize the learning process. An overview is provided in Table II.

Given the reward components, the total reward is calculated using Eq. (5).

$$r_t = \sum r_i \cdot w_i \cdot dt \quad (5)$$

In addition to existing rewards from the literature, we introduced a "Center of Mass" reward to encourage a stable walking gait. This reward calculates the desired centre-of-mass position \mathbf{p}_{xy}^{des} , as the mean xy-components of the feet positions and penalises the squared error from this target, ensuring the centre of mass remains within the support polygon.

Action Space: The position-based controller uses 12 actions to specify target positions for each joint. Our controllers extend actions to adjust the stiffness of the PD controller, ranging from 20 to 60. To study the stiffness adjustments on quadrupedal robots with 12 DoFs, we propose different grouping strategies:

- **Individual Joint Stiffness (IJS):** Predicts stiffness for each joint individually, extending the action space to 24 dimensions.
- **Per Joint Stiffness (PJS):** Groups joints into hip, thigh, and knee categories, predicting one stiffness per group for a 15-dimensional action space.
- **Per Leg Stiffness (PLS):** Predicts one stiffness value per leg, adding four actions for a 16-dimensional space.
- **Hybrid Joint-Leg Stiffness (HJLS):** Combines PJS and PLS by representing stiffness as the outer product of a leg stiffness vector ($\mathbf{k}^l \in \mathbb{R}^4$) and a joint group stiffness vector ($\mathbf{k}^j \in \mathbb{R}^3$), resulting in 19 dimensions.

The damping of the PD controller is set to a fixed relationship to the p-gain, according to Eq. 6.

$$K_D = 0.2\sqrt{K_P} \quad (6)$$

This relationship is inspired by the ratio between PD gains in the works of Gilbert et al., 2023 and Rudin et al., 2022.

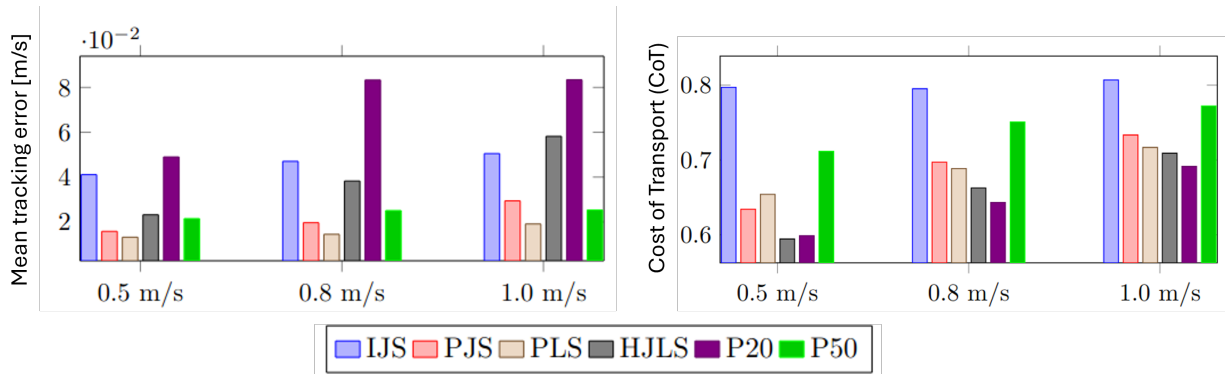


Fig. 3: Comparison of policies in terms of absolute velocity tracking error and cost of transport (CoT).

IV. EVALUATION

In this section, we present the experimental results in both Mujoco-MJX and real-world hardware experiments to answer the following questions:

- Can variable stiffness policies improve velocity command tracking performance?
- Do variable stiffness policies show greater robustness against disturbances?
- Are variable stiffness policies more energy efficient?

A. Baseline

The baseline is formed by position control policies with low stiffness 20, referred to as P20, and high stiffness 50, referred to as P50. These baselines, trained under identical conditions, follow prior choices in Nahrendra, Yu, and Myung, 2023; B et al., 2024 for lower stiffness and Gilbert et al., 2023 for higher stiffness. While Gilbert et al., 2023 used even higher gains, we observed instabilities in training and selected 50 as the upper stiffness. These baselines highlight trade-offs, with each stiffness excelling in specific tasks.

B. Performance on walking and running

We evaluate walking and running performance by measuring tracking errors between the commanded and achieved velocities, a common method used in the works of Joonho et al., 2020. Controllers are tested on eight discrete headings (0° , 45° , ..., 315°) with target speeds of 0.5 m/s, 0.8 m/s, and 1.0 m/s for walking, high-speed walking and running, respectively. Each heading is held for eight seconds, and domain randomisation is turned off to focus on tracking accuracy. Fig. 3 shows the absolute velocity tracking error averaged over the heading directions at different speeds. The comparison indicates that P20 has a significant tracking error, whereas P50 maintains lower. Predicting individual joints in a policy (IJS) demonstrates the highest tracking error. However, our grouped stiffness policies, PJS and PLS, show lower or comparable tracking errors than P50. PLS manages to outperform all other controllers in every speed class.

C. Push recovery

Robustness is evaluated by exposing the locomotion policy to external disturbances. Specifically, force pushes to the robot’s trunk with domain randomisation. The evaluation is performed in the same simulation environment as the training. Push recovery is measured under the following conditions:

- Walking speed: 0.3 m/s
- Force push magnitude: 50 - 300N
- Push duration: 0.1 sec

Pushes are applied randomly in the xy-plane. The robot must walk straight for 5 seconds, with a random push applied between 2.5 and 3.5 seconds. A fall results in failure, while successful recovery and walking for 5 seconds are considered successful. The randomisation of the push event is done to prevent bias due to specific postures.

The success rate for pushes within the magnitude constraints is reported in Table III. Within the push force of 150N (training range), our controller PJS performs best. Above 150N IJS shows the highest success rate, closely followed by PLS and HJS. Since PLS also outperformed the baselines in velocity tracking and shows the second-highest success rate ($< 300N$), we use this policy for further comparison.

Control paradigm	Success Rate (%)				
	$< 100N$	$< 150N$	$< 200N$	$< 250N$	$< 300N$
IJS	100.00	98.73	96.06	93.53	90.44
PJS	100.00	100.00	96.63	89.34	81.64
PLS	100.00	99.66	97.66	92.34	85.65
HJLS	99.83	99.32	97.03	91.58	83.93
P20	99.48	99.07	94.98	89.93	83.08
P50	100.00	99.75	97.20	89.93	81.77

TABLE III: Push recovery success rates within the specified push force magnitudes.

For comparison, we draw a polar scatter plot illustrating the magnitude and angle of the force applied to the robot trunk. We utilise a Support vector machine(SVM) with a radial bias function kernel to classify a maximum recovery boundary. This maximum recovery boundary is used to compare the methods. Figure 4 shows the results of this experiment. All policies show higher resilience in and against the walking direction (0 , 180°). Pushes applied from the side are not well compensated, which is reasonable since we limited the

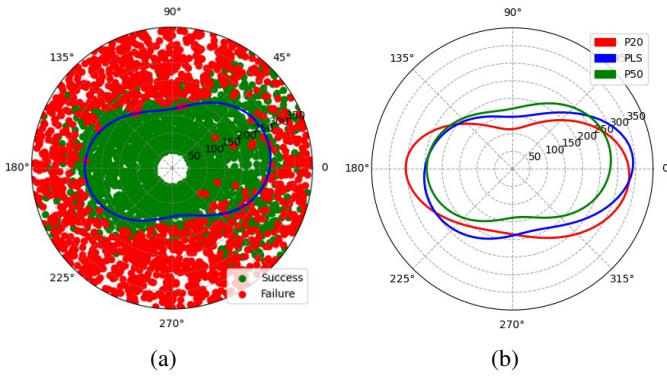


Fig. 4: **Comparison of maximal recoverable force push.** The polar scatter plot (a) shows the outcome of the experiment for specific forces (red=failure, green=success). The SVM, with classification confidence 90%, is used to draw a success boundary in the polar plot (a), which is then used to compare our methodology against the baselines in plot (b).

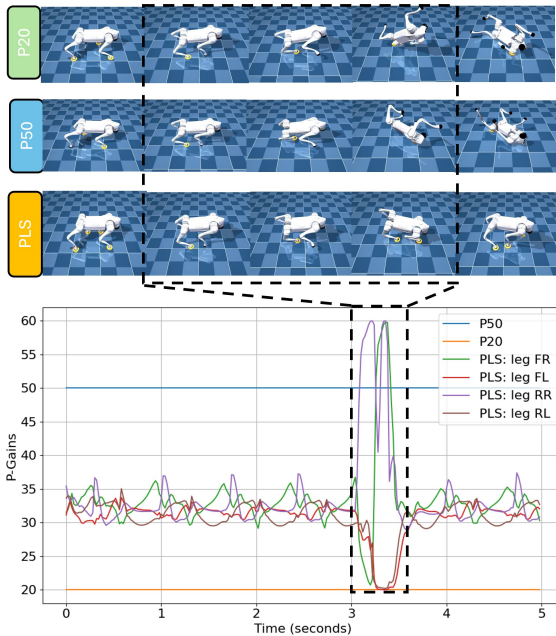


Fig. 5: Policies exposed to left push in simulation and P-gains over time. Push conditions: $t_{push} = 3s$, $t_{duration} = 0.1s$, $F = 190N$, $\theta = 225^\circ$ accounting for the point in time, duration, magnitude and direction at which the push is applied. The force is applied from the frontal left direction. (FR/FL: front left/right, RR/RL: Rear right/left)

hip range to achieve a more natural-looking gait. P50 shows a smaller region than P20. Our policy PLS demonstrates a convex and similar shape to the P20.

Figure 5 further demonstrates how the baseline policies react to a force of 190N applied from the frontal left direction. The graph shows the stiffness values plotted over time for the respective legs. The baseline policies fall, whereas the PLS

manages to recover by adjusting the stiffnesses of the legs. Notably, the legs opposite to the push stiffen way above the maximum stiffness of the high stiffness policy, and the legs towards the push relax. These results demonstrate the superior performance of variable stiffness in this setting.

D. Energy efficiency

Similar to the work of Joonho et al., 2020, we evaluate energy efficiency with the cost of transport (CoT) for different speed classes. They define the CoT as Eq. (7), where M_{total} accounts for the total mass of the robot, τ denotes the measured torques, \dot{q} the joint velocities, g the gravitational acceleration and v for the measured velocity.

$$CoT = \frac{E}{M_{total}gd} = \frac{P}{M_{total}gv} = \frac{\tau\dot{q}}{M_{total}gv} \quad (7)$$

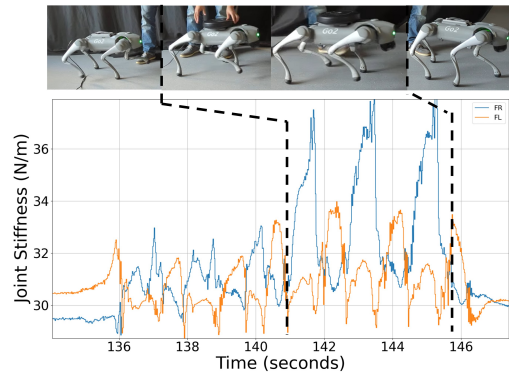


Fig. 6: **Payload experiment:** Adding a 5kg mass during walking to the PLS policy.

We measure this metric applied to the same experiment as described in sec. IV-B. The results are shown in Fig. 3 and reveal mixed results. The lower the CoT, the more energy efficient. Our policies PJS, PLS and HJLS demonstrate lower CoT than P50 but higher than P20. This is also expected as higher stiffness leads to higher torques and, therefore, higher energy consumption. Our policies can adjust their stiffness between 20 and 60; thus, we expect the CoT to be somewhere in between. Lowering the lower border of stiffness compromised gait quality in our experiments. The results validate the expectations. HJLS demonstrates the lowest CoT among our policies and, therefore, the most energy efficient. These results validate the effectiveness of our proposed methodology in grouping the stiffness.

E. Sim-to-real transfer

During hardware deployment, we evaluate the robustness of the learned locomotion by adding a payload or walking over diverse terrains. In training, the policy encounters a randomised payload of up to 3kg. For evaluation, we add a 5 kg payload on the robot during walking and observe increased stiffness while maintaining a proper gait, as seen in

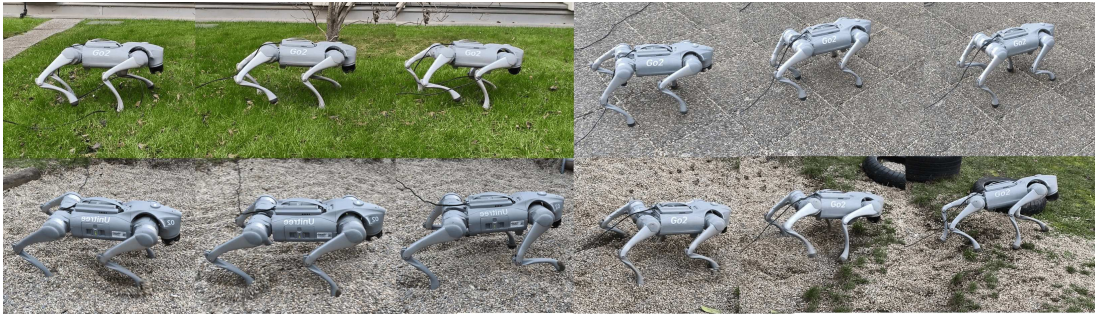


Fig. 7: Despite being trained solely on a flat floor in simulation, we showcase the robot’s ability with our variable-stiffness RL policy to walk robustly on diverse outdoor terrains, such as grass, stones, and sand.

Fig. 6. When the payload is removed, the stiffness decreases accordingly.

We also evaluate our variable stiffness policy in the outdoors to traverse various terrains, although it is trained solely on a flat floor (see Fig. 7). The learned policy demonstrates robustness walking across diverse surfaces, including mud, grass, sidewalks, and pebbles. 7.

V. FUTURE WORK

Our work demonstrates the benefits of variable stiffness. In future works this method could be applied to learn even more different tasks like crouching, hopping stair traversal and imitating motions. As this approach is able to adjust the stiffness this method might also learn these tasks for multiple robot types and combine it into one policy.

VI. CONCLUSION

In this paper, we studied an alternative approach to learning locomotion on a quadruped robot, which uses joint positions alongside stiffnesses as the action space in a reinforcement learning paradigm. Simulation and real-world experiments are conducted to investigate performance on walking and running, as well as push recovery, energy efficiency and sim-to-real transfer. Our policy, which predicts stiffness per leg, outperformed baselines in the robustness test and velocity tracking. On the other hand, individual joint stiffness prediction struggled, underscoring the efficiency of our found groupings. Hardware tests show stiffness adaptation when encountered with payload and robust walking over diverse terrains. Our research highlights the potential of reinforcement learned variable stiffness locomotion and deserves further study.

REFERENCES

- Emanuel, Todorov (2012). “MuJoCo: A physics engine for model-based control”. In: *2012 IEEE RSJ International Conference on Intelligent Robots and Systems*.
- Schulman, John et al. (2017). *Proximal Policy Optimization Algorithms*.
- Jared, Di Carlo et al. (2018). “Dynamic locomotion in the mit cheetah 3 through convex model-predictive control”. In: *2018 IEEE RSJ international conference on intelligent robots and systems (IROS)*.
- Donghyun, Kim et al. (2019). “Highly dynamic quadruped locomotion via whole-body impulse control and model predictive control”. In: *arXiv*.
- Joonho, Lee et al. (2020). “Learning quadrupedal locomotion over challenging terrain”. In: *Science Robotics*.
- Miroslav, Bogdanovic, Khadiv Majid, and Righetti Ludovic (2020). “Learning Variable Impedance Control for Contact Sensitive Tasks”. In: *IEEE Robotics and Automation Letters*.
- Zhaoming, Xie et al. (2021). “Dynamics Randomization Revisited: A Case Study for Quadrupedal Locomotion”. In: *IEEE International Conference on Robotics and Automation*.
- Rudin, Nikita et al. (2022). *Learning to Walk in Minutes Using Massively Parallel Deep Reinforcement Learning*.
- Xinyuan, Zhao et al. (2022). “Variable stiffness locomotion with guaranteed stability for quadruped robots traversing uneven terrains”. In: *Frontiers in Robotics and AI*.
- Donghyeon, Kim et al. (2023). “Torque-based deep reinforcement learning for task-and-robot agnostic learning on bipedal robots using sim-to-real transfer”. In: *IEEE Robotics and Automation Letters*.
- Gilbert, Feng et al. (2023). “Genloco: Generalized locomotion controllers for quadrupedal robots”. In: *Conference on Robot Learning*.
- Laura, Smith, Kostrikov Ilya, and Levine Sergey (2023). “Demonstrating a walk in the park: Learning to walk in 20 minutes with model-free reinforcement learning”. In: *Robotics: Science and Systems (RSS) Demo*.
- Nahrendra, I Made Aswin, Byeongho Yu, and Hyun Myung (2023). *DreamWaQ: Learning Robust Quadrupedal Loco-*

- motion With Implicit Terrain Imagination via Deep Reinforcement Learning*. arXiv.
- Shuxiao, Chen et al. (2023). “Learning torque control for quadrupedal locomotion”. In: *IEEE-RAS 22nd International Conference on Humanoid Robots (Humanoids)*.
- B, Margolis Gabriel et al. (2024). “Rapid locomotion via reinforcement learning”. In: *The International Journal of Robotics Research*.
- Jiaming, Fu et al. (2024). “A Novel Variable Stiffness Compliant Robotic Link Based on Discrete Variable Stiffness Units for Safe Human Robot Interaction”. In: *Journal of Mechanisms and Robotics*.
- Lei, Yu et al. (2024). “A Compact Variable Stiffness Actuator for Agile Legged Locomotion”. In: *IEEE ASME Transactions on Mechatronics*.